ADVANCED MATERIALS
www.advmat.de

Fluidic Ultrasound Generation for Non-Destructive Testing

Benjamin Bühling, Stefan Maack, and Christoph Strangfeld*

Air-coupled ultrasonic testing (ACU) is a pioneering technique in non-destructive testing (NDT). While contact testing and fluid immersion testing are standard methods in many applications, the adoption of ACU is progressing slowly, especially in the low ultrasonic frequency range. A main reason for this development is the difficulty of generating high amplitude ultrasonic bursts with equipment that is robust enough to be applied outside a laboratory environment. This paper presents the fluidic ultrasonic transducer as a solution to this challenge. This novel aeroacoustic source uses the flow instability of a sonic jet in a bistable fluidic switch to generate ultrasonic bursts up to 60 kHz with a mean peak pressure of 320 Pa. The robust design allows operation in adverse environments, independent of the operating fluid. Non-contact through-transmission experiments are conducted on four materials and compared with the results of conventional transducers. For the first time, it is shown that the novel fluidic ultrasonic transducer provides a suitable acoustic signal for NDT tasks and has potential of furthering the implementation of ACU in industrial applications.

1. Introduction

Ultrasonic testing is a widely used tool to gain structural information about various materials. Applications range from medical investigations[1] and trees health determination[2] to production monitoring of composites[3] and reassessment of bridges.[4] If the acoustic propagation velocity of the material is known, measuring the time-of-flight (ToF) of an ultrasonic signal through a specimen enables the detection of embedded objects, cracks or phase boundaries acting as reflectors. Depending on the measurement task, different wave types, such as longitudinal, transverse, plate or surface waves, can be used. For known specimen dimensions, ToF measurements are used to determine the acoustic propagation velocity of different waves and to infer further properties of the specimen. For example, the propagation velocity of longitudinal waves has been found to be related to fat depositions in rat livers,[5] particle content in two-phase suspensions,[6] food properties,[7,8] load,[9] and residual stress in polymers,[10] the curing process of resins,[3,11] the hydration of mortar,[12] and the aggregate content of concrete.[13]

Most commonly, the sending and receiving ultrasonic transducers are coupled directly to the specimen surface[14,15] or a liquid coupling medium is used.[16,17] This procedure minimizes the loss of acoustic energy due to a mismatch of the characteristic acoustic impedance at the interface between transducers and specimen. Direct coupling at each measurement point is time consuming, so that immersing the transducers and specimen into the coupling agent can be used to increase flexibility and measurement speed.[18–20] However, liquid immersion may be restricted, e.g., for very large specimens such as concrete infrastructures,[21] air immersed particles,[22] sensitive specimens such as art works[23] and liquid foams,[24] or when monitoring processes in harsh ambient conditions.[11,25] In these cases, it is preferable to use the ambient fluid, i.e., air, as a couplant. While air-coupled ultrasonic (ACU) methods are considered the optimal choice in terms of time efficiency and of coupling feasibility,[26] impedance mismatch losses at the interfaces between transducer, air and specimen are high, amounting to −110 dB for materials with high acoustic impedance such as concrete.[27] Several approaches have been pursued to minimize these losses. Thus, matching layers have been applied at the interface of the common piezoelectric and capacitive transducers to air,[28,29] or alternative ultrasound generation methods have been used to completely cut out this interface. The methods include ultrasound generation by thermoacoustic[30,31] and plasma transducers,[32,33] as well as wave generation inside the specimen by X-rays,[34,35] microwaves,[36,37] or laser heating.[38,39]

In this work, a novel approach to ultrasound generation based on fluidic transducers[40,41] and its practical application for non-destructive testing (NDT) tasks is described. The signal itself is generated by an instationary air flow inside a fluidic switch, in contrast to approaches that use fluids as waveguides[18,42] or as intermediaries to determine the strength of materials.[43] Enabling the generation of acoustic pulses is a significant development from previous approaches for aeroacoustic ultrasonic sensing devices, that were only able to generate continuous tones.[44,45] Since the acoustic signal is generated by the same medium that is emitted to, the characteristic impedance losses disappear when the pulse leaves the transducer into the ambience. The fluidic ultrasound generating part of the transducer is

B. Bühling, S. Maack, C. Strangfeld
Department 8 "Non-Destructive Testing"
Bundesanstalt für Materialforschung und -prüfung
Unter den Eichen 87, 12205 Berlin, Germany
E-mail: benjamin.buehling@bam.de

The ORCID identification number(s) for the author(s) of this article can be found under https://doi.org/10.1002/adma.202311724

DOI: 10.1002/adma.202311724

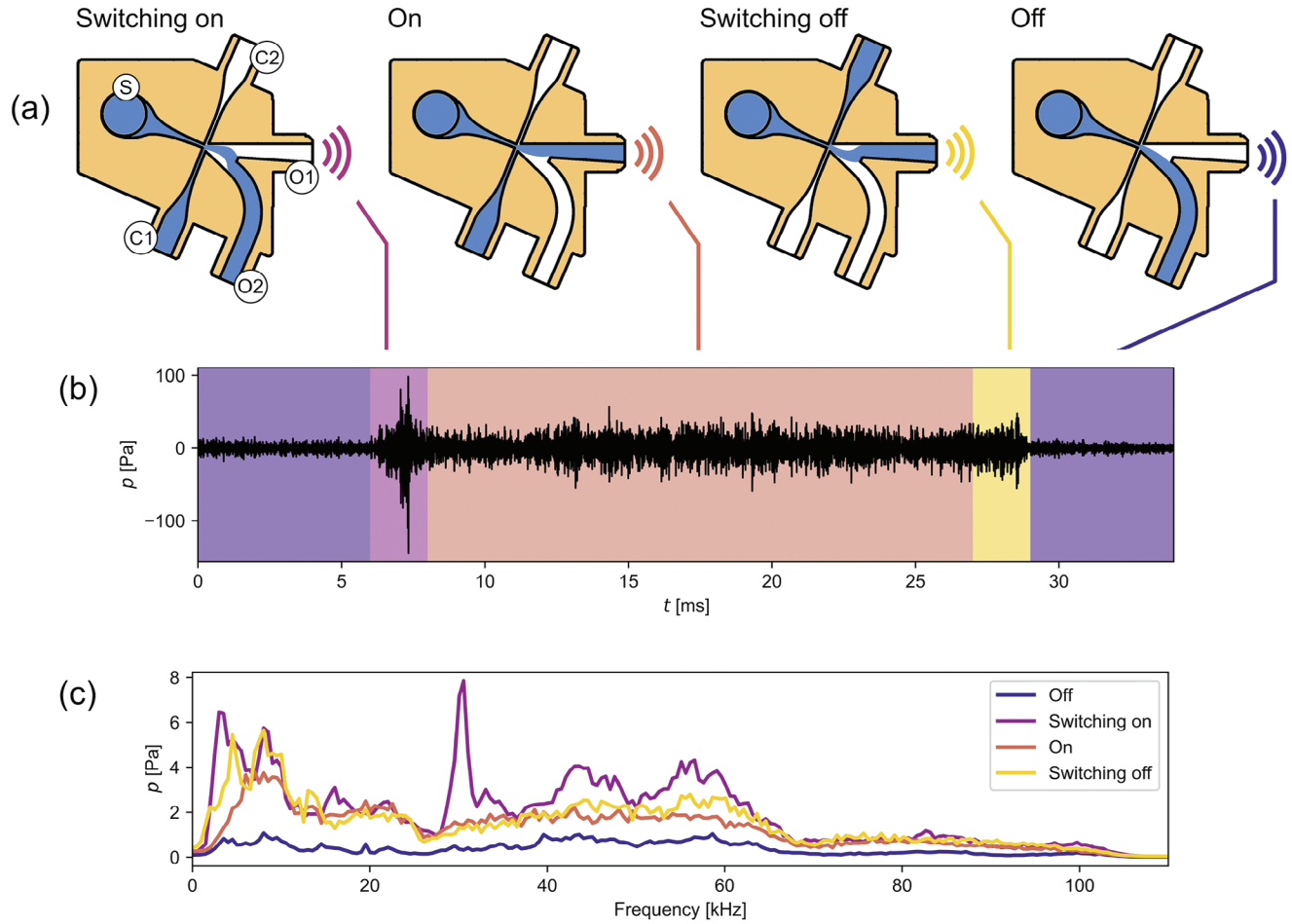

Figure 1. a) Flow switching process inside the fluidic transducer. S – supply port, C1 – control port 1, C2 – control port 2, O1 – outlet 1, O2 – outlet 2. b) Exemplary microphone time signal in which the stages of the flow switching process are highlighted. c) Frequency domain of the highlighted regions showing the distinct frequency content of the sound generated during the process of *switching on*.

a purely static set of channels through which the flow is guided. Thus, the material can be chosen according to both working fluid and environmental properties, making it resistant to harsh environments while retaining their functionality as previous fluidics research has shown. These environments may include high temperature,[46,47] radiation,[48,49] or corrosive atmospheres.[50,51] Additionally, the sound generating part of the transducer requires no moving parts, making it maintenance-free, provided the working fluid is clean enough to avoid particle aggregation on inside the channels.[52] The transducer was developed for use in NDT in civil engineering, where transmitter robustness and low ultrasonic frequencies are specific requirements. However, its principle resilience to harsh environmental conditions make it a suitable option for other ultrasonic generation applications. In this paper, the applicability of a fluidic ultrasound setup for NDT tasks is demonstrated in a laboratory setting and compared with conventional methods. In addition to the novelty of the fluidic transducer, being able to generate high-amplitude transient ultrasonic pulses using only an instationary air jet, this paper shows for the first time the possibility to derive useful material properties by using the device in conjunction with a refined optical ultrasonic sensing setup.

2. Results and Discussion

2.1. Fluidic Transducer

The operating principle of the fluidic transducer is equivalent to a bistable fluidic switch[47,53] and is outlined in **Figure 1a**. In the initial state, a pressurized fluid is connected to the main inlet of the device and leaves it through one of the outlet channels (O1 or O2). The active outlet channel can be controlled by allowing an additional pressurized fluid to enter the device through one of the control ports (C1 or C2). When O2 is the active outlet and C1 is opened, the main flow switches to O1. The main flow is switched back to O2 by closing C1 and opening C2. Once the switching of the outlet channels is complete, the flow in this configuration remains stable until the opposite control port is activated. During this switching process, strong sound pressures can be attained which originate from the supersonic flow inside the device, the exiting free jet and the flow instabilities during the switching process. The latter causes significantly higher acoustic pressure amplitudes than the other sources over a wide frequency range. In this study, only the sound emitted from O1 is used. Therefore, the device is described as *on* when the flow exits

O1 and *off* when it exits O2. The ultrasonic signal generated by the fluidic transducer is shown in Figure 1b. The four parts of the fluidic switching cycle are reflected in the time signal (Figure 1b). Their average frequency content at location $(x, y) = (110, 0)$ mm is shown in Figure 1c. During the process of *switching on*, three distinct frequency peaks can be seen at 30.5 , 43.5 , 56.5 kHz. During *switch-off*, the first of these peaks is absent. In stable *on* and *off* states, the transducer shows none of these peaks.

Comparing the ultrasonic signal of the fluidic transducer to that of a piezoelectric transducer (see Section S.2, Supporting Information) or other recent ACU transducers shows a number of unexpected features. First, the signal is significantly longer than the low number of periods generated by the ringing of a piezoelectric transducer or than the single spike burst generated by a thermo-acoustic transducer.[30] While Figure 1b shows a time frame of 35 ms, the characteristic ultrasonic frequencies generated by the transducer were found solely at the time of switching *on* the flow, when the sound pressure peaked. Thus, this part of the signal, which is still in the range of a few hundred milliseconds, can be considered as the main signal and will be referred to as the pulse in the following. While Figure 1c shows the mean frequency content of 40 pulses, the frequency content of each individual pulse varies. The multiple peaks are a feature that is distinguishes the pulse of this transducer from those of common piezoelectric or capacitive transducers.[26] The variations of the frequency content of the individual pulses can be considered as inherent random phase and frequency modulation.[54] Analyzing fluidic pulses in this framework allows comparison of signal length with other pulse compression techniques, such as chirps.[55] Although the random modulation technique is inferior to current pulse compression techniques, it has the advantage of not requiring additional modulation control when operating the fluidic transducer. Furthermore, this modulation is not restricted to the 1 to 2 ms pulse range of the time signal. As proposed in previous publications on modulation in ultrasound,[56,57] it is possible to extend the time window used for correlation to the flow noise following the initial pulse in the transducer *on* state. While it does not contain all the frequency peaks of the pulse range, it still contains considerable acoustic energy that contributes to effective pulse compression, even if not to the same extent as the pulse itself. Analysis of the usability of fluidic signals for NDT is based on a 2 ms time window containing the first pulse of the fluidic transducer. This signal duration is comparable to the time windows used in previous pulse compression studies with chirped signals.[58–60] Extending the correlation time window further into the lower amplitude flow noise regime results in slightly improved cross-correlation results in terms of signal-to-noise ratio, but increases both measurement time and computational effort.

The directivity of the transducer is shown in **Figure 2** for the *switch-on* process. Close to the horn mouth, a mean ultrasonic pressure amplitude of 320 Pa is reached when the fluidic transducer is switched *on* and 140 Pa when it is switched *off*. At a distance of 110 mm, where the subsequent measurements were conducted, the mean centerline amplitude at switching *on* is 140 Pa. At this position, the ultrasonic field has a width of 90 mm at half maximum amplitude, ensuring a high directivity of the refracto-vibrometric measurements (see Section S.1, Supporting Information). The ultrasonic field given in Figure 2, shows a more directive sound field with a higher maximum sound pressure compared to the almost spherical radiation of the baseline transducer.[40] This can be attributed to the horn at the outlet, which reduces radiation impedance mismatch at the transducer outlet and increases the directivity through an increased outlet diameter. The resulting acoustic power of the transducer amounts to 0.23 W, which is about four times the power of the piezoelectric ACU reference transducer (see Section S.3, Supporting Information). The ultrasonic field of the secondary pulse generated when the flow is switched *off* has a lower peak sound pressure and is briefly discussed in Section S.4 (Supporting Information). Additionally, the horn acts as a diffuser for the high-velocity flow exiting the device. As a secondary effect, the horn therefore enables the application of the fluidic transducer to sensitive specimens as it prohibits a high velocity mass flow to impinge on the specimen surface.[61]

2.2. Procedure

Due to the pressure amplitude generated by the fluidic transducer, it is expected that the signal can penetrate specimens at considerable depth. Since the longitudinal acoustic velocity can be related to various material parameters of the specimen, this property was chosen as the quantity to be measured. For this purpose, the ToF of the signal was measured in a fully optical through-transmission setup (see **Figure 3**a) based on a recently introduced method[62] that has been shown to achieve a ToF accuracy of less than 1 µs for transducer working distances larger than 40 mm. Two laser Doppler vibrometers, LDV 1 and LDV 2, are used to record the ultrasonic signal before entering the specimen and at its back wall, respectively. The resulting signals are then shifted and cross-correlated to obtain the ToF, as detailed in the experimental section. This approach refines the previously published through-transmission setup,[62] which employed only one LDV and one accelerometer, in order to allow true contact-free ToF measurements without requiring prior knowledge about the ambient speed of sound. The longitudinal velocity was then calculated from the ToF with knowledge of the specimen thickness. In order to assess the applicability of the fluidic transducer to a broad range of applications, four materials with various thicknesses were investigated. Two of these were the building materials concrete and wood, since the transducer was originally designed for testing application in civil engineering. Contrary to the other materials investigated, wood, and wood-based materials are anisotropic. To limit the scope of the investigation, only the transverse propagation direction[63] was chosen. To investigate the applicability to biological specimens, a block of ballistic gel was tested. The sound velocity of this material is comparable to that in various tissues[64] and has been used for the fabrication of ultrasound phantoms.[65–67] The fourth material is cast polyamide PA6, a polymer that is often used as a reference case for ultrasonic testing.[68–70] **Table 1** provides a summary of the specimens investigated. The results were compared with those of a commercial piezoelectric ACU transducer, using the same all-optical measurement setup as for the fluidic transducer, and with those of a commercial piezoelectric contact transducer. In general, the longitudinal acoustic velocity of a material is independent of the transducer used, so besides demonstrating the

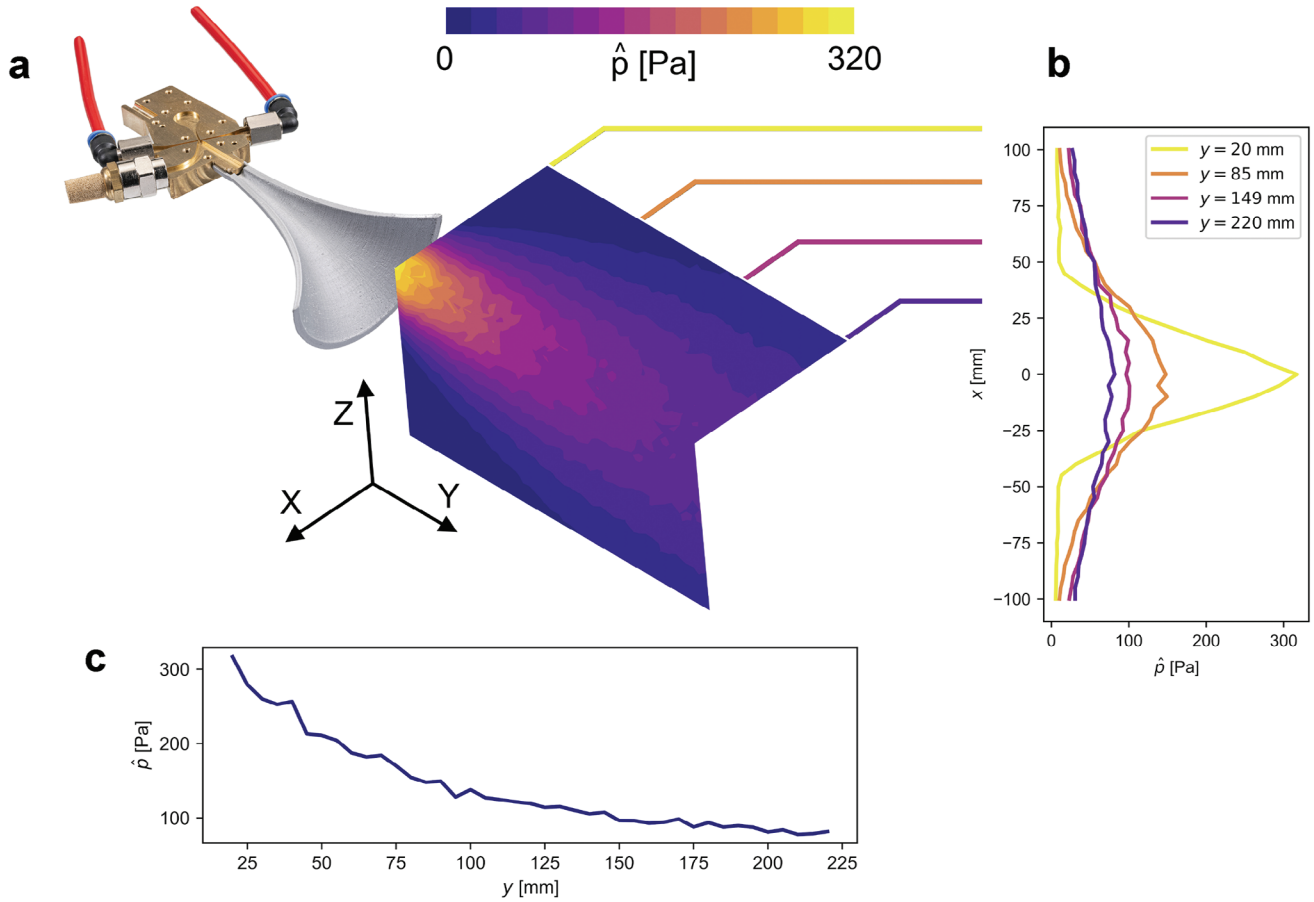

Figure 2. a) Ultrasonic field of the fluidic transducer, where $\hat{p}$ is the mean peak pressure. b) Radial distribution of $\hat{p}$ at various axial positions y. c) $\hat{p}$ distribution along the acoustic axis.

applicability of the fluidic transducer for NDT tasks, comparing the results will give insight into the performance of the optical sensing approach compared to contact measurements. Also expected are conclusions about the performance of the fluidic ACU transducer compared to the piezoelectric ACU transducer.

For each specimen, 100 individual pulses were recorded and evaluated using the matched filter approach outlined in the experimental section. The correlation results were then averaged to find the resulting ToF. Five individual examples for the resulting correlation outputs and the averages from all 100 outputs are given in Figure 3b–i for a subset of the specimens tested. Results obtained for all specimen using the piezoelectric and fluidic transducers are given in Figures S6 and S7 (Supporting Information), respectively. The results show that there is some variation in the individual correlation results, which is greater for the concrete specimen than for the other specimens. When the multiple correlation results are averaged, the correlation result converges. This raises the question of how many individual measurements must be averaged until the correlation output converges. Without considering the corresponding sound velocities, the number of measurements was evaluated that was required for the ToF to lie consistently within ±2.5 % of the final ToF, which was obtained using the total number of 100 pulses. To account for the stochastic variations in the individual correlation outputs, this convergence analysis was executed on 100 permutations of the correlation data from each specimen and ACU transducer combination. Figure 3j shows the results from this analysis, while the underlying distributions are shown in Figures S4 and S5 (Supporting Information).

For most specimens, the fluidic transducer requires more individual pulses to be averaged than the piezoelectric transducer. In general, the most repetitions were required for the concrete specimens, both using the fluidic and the piezoelectric transducer. Except for specimen C80 with fluidic actuation, the numbers of required repetitions increase with specimen thickness, attributed to increasing scattering noise and attenuation. For fluidic measurements at two specimens, C240 and P312, the results converge late, requiring almost all of the measured pulses. This indicates that either more pulses are required to faithfully measure the ToF or that the SNR in these measurements is so low that no stable ToF can be determined. For most other non-concrete specimens, a single digit number of measurements was needed to achieve convergence. The piezoelectric transducer converged immediately for all non-concrete specimens. Concrete and polyamide have the highest specific acoustic impedance of the materials tested in this study, which results in the lowest transmitted acoustic energy. Thus, the influence of noise on the correlation result is greater. The convergence results show that

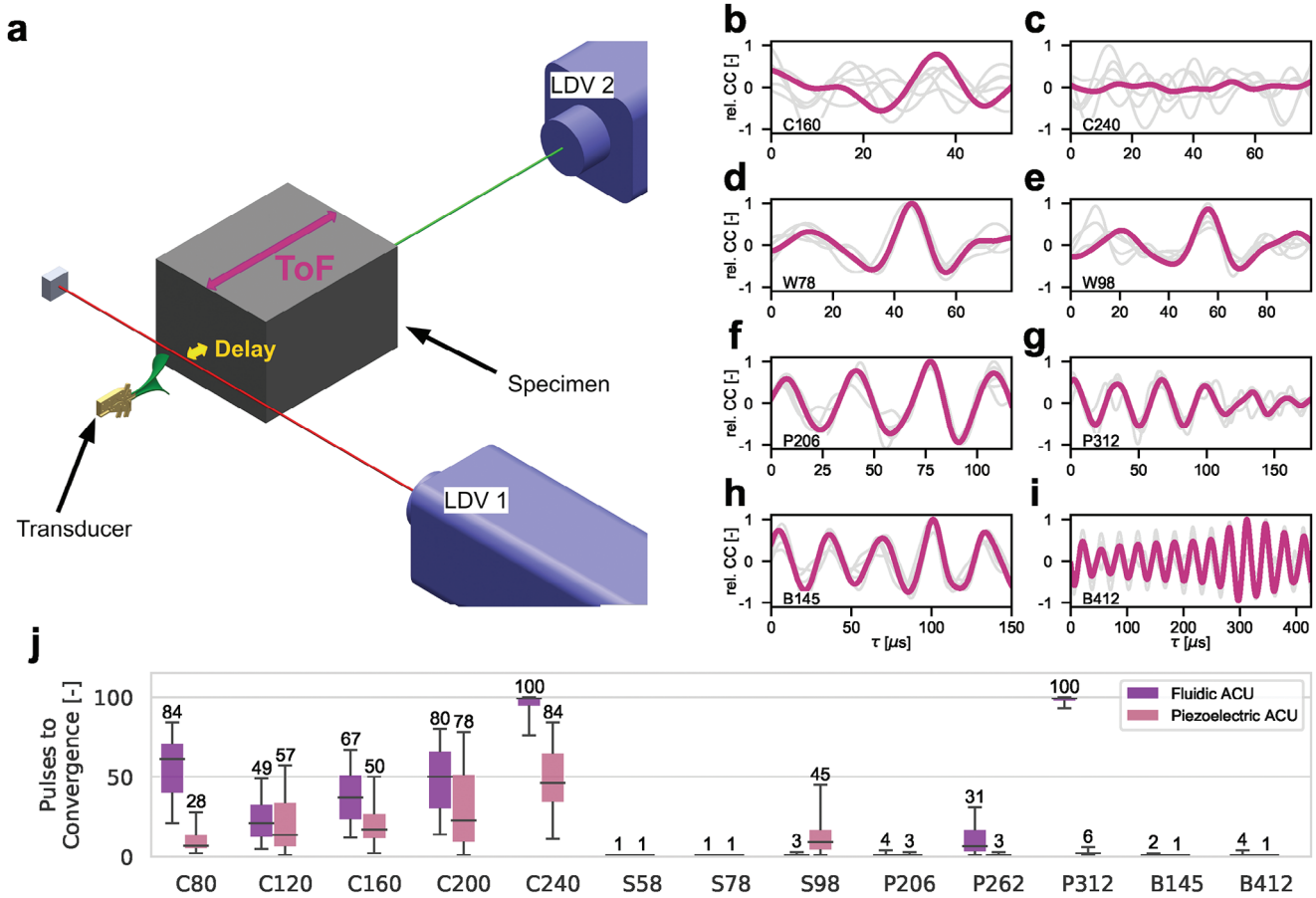

Figure 3. a) Measurement setup used in this study. After the acoustic pulse exits the transducer, it propagates through air before entering the specimen. To obtain the ToF through the specimen, the delay resulting from the travel time through the air has to be subtracted from the overall ToF. b–i) Exemplary cross-correlation outputs obtained using the fluidic transducer. The gray lines are the first five individual cross-correlation outputs, the magenta lines are the mean cross-correlation outputs from 100 measurements. j) Measurements needed for the maximum of the cross-correlation to converge. The whiskers refer to the 5th and 95th percentiles of the respective distributions. The annotated numbers refer to the 95th percentiles. Specimens are abbreviated using the initial letter of their material followed by their thickness in mm, e.g. C160 is the concrete specimen with thickness of 160 mm. All specimens used in this study are tabulated in the experimental section.

the high acoustic pressure generated by the fluidic transducer cannot fully compensate for the influence of its diverging ultrasonic field, reducing the usable acoustic energy arriving at the receiver. However, in the lower acoustic impedance materials, the radiation characteristics of the proposed transducer are sufficient to obtain results with a small number of repetitions.

The measurement method described above has been employed in a laboratory environment only and imposes limitations for in situ measurements. The operability of the fluidic transducer is tied to the availability of pressurized air. While compressed air is already provided for various processes in many laboratories and production facilities, in other settings there might be a need to provide a compressor or an air-containing pressure vessel to operate the transducer. Furthermore, the use of LDVs for sensing requires optical access to the specimen and a vibration-free mount of the devices, which can be provided in a laboratory environment but may be challenging to achieve in factory or outdoor application. While the fluidic transducer is robust to

Table 1. Materials tested in this study and a selection of literature values for their longitudinal sound propagation velocity c_L and mean longitudinal sound propagation velocity $\bar{c}_L$ used to determine the time interval in which the cross-correlation is evaluated.

Material	Through thickness [mm]	Specimen shape	c_L [ms^{-1}]	$\bar{c}_L$ [ms^{-1}]
Concrete	80, 120, 160, 200, 240	Step-shaped block, with 5 steps of 400 mm × 400 mm width	4200...5000[13,71]	4600
Spruce	58, 78, 98	3 timber beams each of 200 mm × 400 mm width	1146...1850[72–74]	1500
Polyamide 6	206, 262, 312	Single block with the dimensions 206 mm × 262 mm × 312 mm	2635...2653[68,75]	2645
Ballistic gel	145, 415	Single block with the dimensions 145 mm × 145 mm × 415 mm	1424...1470[66,67,76]	1450

Figure 4. Measurement results of the fluidic transducer compared to the piezoelectric and contact transducer. The specimens are abbreviated using the initial letter of their material followed by their thickness in mm, e.g., C160 is the concrete specimen with a thickness of 160 mm. All specimens used in this study are tabulated in the experimental section. a) ToF. b) Longitudinal velocity c_L. The bar referring to the fluidic transducer results for specimen P312 (*) is cropped. The actual velocity is calculated to be 156000 ms^{-1}. c) Peak-to-peak ratio (P2P) of the cross-correlation output. The ∞ sign for the P2P of the fluidic transducer transmitting through the first three concrete specimens indicates that no second peak was found, so the P2P would approach infinity. Data from the contact transducer is not included as the P2P measure is applicable only to the ACU measurements.

harsh environments, great care needs to be taken to also adapt the peripheral equipment to those environments. It has also been shown that the sensing method used in this study requires multiple averaged ultrasonic pulse correlations to obtain a converged ToF result. The resulting increase in measurement time is expected to build up further in presence of additional noise sources in non-laboratory environments. Further research is needed to improve the employed methods so that an in situ use is more easily facilitated.

2.3. Time-of-Flight Measurements

The measured ToFs and velocities obtained by applying the described method are shown in **Figure** 4a, b, respectively, and detailed in Table S1 (Supporting Information). Qualitatively, the velocities measured by the different transducers agree well for most specimens. However, there are a number of notable exceptions. For the concrete specimens and two of the spruce specimens, the ACU measurements consistently show lower velocities than the contact measurements, which corresponds to longer ToFs. For heterogeneous materials, two effects have been described to cause ToF deviations. First, the ToF overestimation can be caused by different paths taken by the signal through the materials, as argued by Purnell et al.[77] and Berriman et al.[78] who encountered significant TOF deviations when comparing ACU and contact ultrasound measurements on concrete. When the signal is transmitted from the air to the specimen, it tends to couple into the portion of the material with lower specific acoustic impedance. In concrete, this is the cement instead of the aggregates. This results in a path of propagation that is longer than the direct path to the receiver. Second, both concrete[13,79] and wood[80,81] exhibit dispersive behavior, characterized by reduced acoustic velocity for lower frequency signals generated by the ACU transducers.

A third error source is not limited to heterogeneous materials, but to specimens that are slim in the off-axis direction, such as the long side of the ballistic gel specimen. The directivity of the transducer influences the cross-correlation result by reflections inside the specimen. The ultrasonic waves generated by the fluidic transducer presented in this study, contrary to those from the piezoelectric ACU transducer, cannot be considered as plane waves. Thus, reflections on the boundaries of the specimen arriving later at the receiving sensor than the direct wave may cause a higher correlation result than the direct wave, leading to an erroneous ToF pick. However, these error sources do not explain the large velocity measured with the fluidic transducer through the thickest dimension of the PA6 specimen (P312), the cause of which remains unclear. The non-convergence of the ToF

(Section 2.3) can be interpreted as an early indicator of these faulty results. This is also the only significant negative ToF deviation of the fluidic transducer from the contact measurements.

The ToF deviation of the fluidic measurements compared to the contact measurements was within 5 µs for all specimens except the thinnest spruce specimen (S58) and the thickest side of the ballistic gel (B412). For these two exceptions, the deviation was still within one period of the dominant 30 kHz wavelength. The resulting deviations of the measured longitudinal velocity depended strongly on the specimen thickness. Thus, the measured velocity deviations were high for the thinnest concrete specimens (21.8 %) and for the thickest side of the ballistic gel block (9.7 %), although the ToF deviation by the latter was seven times higher. Generally, the measured longitudinal velocities shown in Figure 4b were comparable for all transducer types, except for the aforementioned P312 specimen. In detail, there were cases where one transducer deviates moderately from the others. Apart from the fact that deviations were more frequent for heterogeneous materials, these outliers showed no discernable trend.

The results presented in Figures 4a,b show that this signal is suitable for measurement of longitudinal acoustic velocity in transmission mode. The identified ToFs of the fluidic transducer agreed well with the reference measurements except for two specimens. Except for the largest propagation distances in polyamide and the ballistic gel (P312 and B412), the ToF difference between the fluidic measurements and the reference measurements was smaller in homogeneous materials than in heterogeneous ones.

2.4. Output Quality

The peak-to-peak ratio (P2P) of the cross-correlation output, given as the ratio of the cross-correlation maximum to the secondary positive peak in the observed time interval, was chosen as the measure of output quality. The P2P is based on the peak sidelobe ratio (PSLR), which is often used as a quality measure in radar technology.[82] While the PSLR is a measure calculated from the autocorrelation of the transmitted signal, the P2P of the cross-correlation result indicates how clearly the correlation maximum can be distinguished from later peaks. These peaks can be caused by multiple reflections or alternative sound propagation paths in the actual specimens. Figure 4c shows that the P2P of the correlation results from the fluidic transducer measurements is in all cases equal or superior to the results with the piezoelectric transducer. Only for the specimens that exhibit large ToF deviations and thus seem to be already faulty, differences in the results can be seen. For the thinnest portions of the concrete specimen, no P2P values could be calculated because there was only one correlation peak in the time frame investigated, leading to a theoretical P2P of infinity.

The generally higher P2P value of the fluidic transducer compared to the piezoelectric transducer is caused by the inherent pulse compression of the transducer.[54] Since the piezoelectric transducer produced a very reproducible narrowband signal, the correlation result appears as a short narrowband wave packet containing multiple local maxima (see Figure S4, Supporting Information). The amplitudes of the maxima are close to each other, resulting in a low P2P. The signal of the fluidic transducer did not produce a packet-like result, but a single prominent peak. Depending on the investigated time frame of the correlation output, this peak can even be singular, as in the case of the thin concrete specimens. Since the emitted acoustic wave cannot be considered as a plane wave, most of the acoustic energy entering the specimen is refracted off the direct sound path to the backwall vibrometer. Thus, the sensed particle velocity has a low signal-to-noise ratio, requiring averaging of the correlation results. While this averaging aids the convergence of the calculated ToF, i.e., the time shift at the cross-correlation maximum, it does not significantly increase the piezo transducer's P2P, which is limited by the waveform. However, the P2P of the fluidic transducer is additionally increased, as random noise terms are canceled out. The P2P of the fluidic transducer then converges like the ToF, as only systematic sources of correlation maxima remain.

3. Conclusion

A novel air-coupled ultrasound transducer for non-destructive testing based on the design of a bistable fluidic switch is presented. This fluidic transducer uses pressurized air to generate an ultrasonic pressure signal in the ambient air without the impedance mismatch losses common to conventional transducers. Due to its simple and rugged design, it can theoretically withstand harsh environments that are outside the operating conditions of conventional ultrasonic transducers. The signal has an average peak acoustic pressure of 320 Pa and a frequency range of up to 60 kHz. Transducer performance for ToF measurements in through-transmission was investigated for various homogeneous and inhomogeneous materials and compared to a conventional piezoelectric air-coupled transducer and a conventional contact transducer with comparable center frequency. While the results showed deviations between all transducers, the measured acoustic velocities fell largely within the expected range. Due to the inherent random modulation of the fluidic pulses and the high acoustic pressure, the peak-to-peak ratio of the cross-correlation results was generally higher and the ToF results converged as well or faster than the piezoelectric air-coupled transducer. The results show that the fluidic transducer is suitable for through-transmission measurements of various technically relevant materials. This first proof of usability and competitiveness enables the exploration of further use cases that require robust ultrasound generation. Beside determining the environmental limits of this transducer, further research will be directed at optimizing the generated waveform in terms of length and frequency content to broaden the range of realizable measurement tasks. Developing alternative receiver strategies will alleviate the dependence on optical access and vibrational sensitivity of the currently employed LDVs and reduce the barrier to adaption in industrial settings by lowering the cost of equipment.

4. Experimental Section

Fluidic Transducer Operation: The fluidic transducer was operated in the mode described in a previous study[83] and shown in Figure 3a. A constant pressure of 1.8 bar was applied to the main inlet. The control valves (MHJ10 by Festo, Germany) were operated for 15 ms each to initiate the switching process and subsequently reset the fluidic state, at a pulse repetition rate of 4 Hz. The control flow tube had a length of 250 mm. An

additively manufactured exponential horn (length $\ell = 86.6$ mm and exponent $\epsilon = 36.6$) was mounted on its main outlet O1, while the secondary outlet O2 was equipped with an AMTE brass silencer (Festo, Germany).

Microphone Averages: The ultrasonic field of the fluidic transducer was investigated with a calibrated microphone (MK301 measurement microphone capsule with MV302 preamplifier by Microtech Gefell, Germany). These data were recorded using a USB-6361 DAQ (National Instruments, USA). The average peak sound pressure was determined using 40 individual pulses at each measurement point. The accuracy of these averaged maximum pressure values was estimated to be about ±5%.[83]

Materials: The materials used in this study are listed in Table 1 together with the dimensions of the specimens and the literature values for the respective sound velocities. The time window $[\tau_l, \tau_u]$ in which the cross-correlation maximum occurs was limited to both reduce the computation time and exclude cross-correlation maxima caused by the airborne sound interacting with the back-surface vibrometer. The lower limit of this time windows was set to $\tau_l = 0$ µs, which would correspond to an infinite longitudinal velocity or an infinitely thin specimen. The upper limit was set to $\tau_u = 1.5d/\bar{c}_L$, where d is the specimen thickness and $\bar{c}_L$ is the center velocity of the material under investigation (see Table 1). This upper limit allowed an underestimation of longitudinal velocity by 33 % and an underestimation of the material thickness by 50 %. In practical applications where more precise a priori knowledge was included in the process, the time window for maximum search may be reduced significantly.

Contact Measurements: Contact ToF measurements were conducted with two single 100 kHz S0208 piezoelectric transducers (ACS, Russia) for sending and receiving. They were coupled to the specimen using a thin layer of petroleum jelly. The contact transducers were excited using a A1220 Monolith ultrasonic tester (ACS, Russia) and sensed with the same device at a sampling rate of 1 MSs^{-1}. The first maximum of the signal was chosen to determine the ToF.

Air-Coupled Measurements: ACU ToF measurements were conducted using two laser Doppler vibrometers (Nova Sense by Optomet, Germany, and OFV 3001 vibrometer controller with OFV 303 laser head from Polytec, Germany) and a M2p5966-x4 measurement card (Spectrum Instrumentation, Germany) with a sampling rate of 20 MSs^{-1} for recording. The measurement setup was based on a previous study.[62] While one vibrometer (LDV1) was used in refracto-vibrometry (RV) mode, the other (LDV2) was aimed at the back surface of the specimen. When an LDV laser beam was used as an acoustic sensor in RV mode, it was sensitive to all acoustic signals that pass the laser beam perpendicularly. Therefore, the LDV recorded the incoming signal from the transducer and the signal reflected from the specimen surface. Autocorrelation of the signal from LDV1 resulted in a secondary peak corresponding to twice the time delay between the acoustic signal passing the laser beam and entering the specimen. The ToF through the specimen could then be determined by cross-correlating the two LDV signals and subtracting the in-air time delay and a separately determined hardware delay.

Contrary to the study that introduced this measurement technique,[62] the LDVs in the current investigation did not measure the same physical quantities. LDV1 in RV operation sensed the temporal change in refractive index $n(t)$ so that the signal $s_1(t) = s_1(\partial n/\partial t)$. In the pressure range considered here, $n(t)$ could be considered as a linear function of the acoustic pressure p,[84] so that $s_1(t) = s_1(\partial p/\partial t)$. The second vibrometer measured the particle velocity at the specimen surface. This was in phase with $p(t)$ in far-field condition. Thus, $s_1(t)$ was integrated before correlation to correct for the $\pi/2$ phase shift between sound pressure and particle velocity.

The hardware delay for the settings used in this experiment was determined to be $t_d = 160$ µs by focusing the vibrometers on the same spot of a rigid surface and vibrating them with a small hammer. The in-air time delay was calculated individually for each measured ultrasonic pulse so that small changes in $c_{L,air}$ were corrected for each instant.

A piezoelectric ACU transducer NCG100-S63 (Ultran Group, USA) with a center frequency of 80 kHz[40,62] was used for comparison with commercial systems. The same measurement setup was used. All signals were band-pass filtered using a Butterworth filter in the [20,100] kHz range. The distances from the surface to the transducers and the RV laser beam were 110 and 50 mm, respectively. Although the transducer positioning influences the achievable sound pressure of the ultrasonic pulse entering the specimen, depending on the transducer directivity, the same transducer positions were chosen to obtain comparability for practical applications.

Supporting Information

Supporting Information is available from the Wiley Online Library or from the author.

Acknowledgements

This research was funded by the German Federal Ministry for Economic Affairs and Climate Action (BMWK) under the Zentrales Innovationsprogramm Mittelstand (ZIM) grant number ZF4044222WM7.

Open access funding enabled and organized by Projekt DEAL.

Conflict of Interest

The authors declare no conflict of interest.

Data Availability Statement

The data that support the findings of this study are available from the corresponding author upon reasonable request.

Keywords

aeroacoustics, air-coupled ultrasound, fluidics, harsh environment, laser Doppler vibrometer, non-destructive testing

Received: November 6, 2023
Revised: January 4, 2024
Published online:

[1] T. L. Szabo, *Diagnostic Ultrasound Imaging*, vol. *1*, Academic Press, Burlington, MA, USA **2004**.
[2] L. Espinosa, J. Bacca, F. Prieto, P. Lasaygues, L. Brancheriau, *Acta Acust. United Ac.* **2018**, *104*, 429.
[3] A. Palevicius, E. Dragasius, R. Bansevicius, M. Ragulskis, in *Proc. SPIE*, vol. *5384*, SPIE, Bellingham, WA, USA **2004**, pp. 71–79.
[4] S. Küttenbaum, T. Braml, A. Taffe, S. Keßler, S. Maack, *Struct. Concr.* **2021**, *22*, 2895.
[5] H. Kumagai, K. Yokoyama, K. Katsuyama, S. Hara, H. Yamamoto, T. Yamagata, N. Taniguchi, N. Hirota, K. Itoh, *Ultrasound Med. Biol.* **2014**, *40*, 2499.
[6] J. Fan, F. Wang, *Rev. Sci. Instrum.* **2021**, *92*, 091502.
[7] E. Corona, J. V. Garcia-Perez, T. E. Gomez Alvarez-Arenas, N. Watson, M. J. W. Povey, J. Benedito, *J. Food Eng.* **2013**, *119*, 464.
[8] S. O. Kerhervé, R. M. Guillermic, A. Strybulevych, D. W. Hatcher, M. G. Scanlon, J. H. Page, *Food Control* **2019**, *104*, 349.
[9] F. Lo Savio, M. Bonfanti, *Polym. Test.* **2019**, *74*, 235.
[10] D. Jia, G. Bourse, S. Chaki, M. F. Lacrampe, C. Robin, H. Demouveau, *Res. Nondestruct. Evaluation* **2014**, *25*, 20.
[11] F. Lionetto, A. Maffezzoli, *Materials* **2013**, *6*, 3783.
[12] D. G. Aggelis, T. P. Philippidis, *NDT E Int.* **2004**, *37*, 617.
[13] T. P. Philippidis, D. G. Aggelis, *Ultrasonics* **2005**, *43*, 584.
[14] M. Krause, U. Dackermann, J. Li, *J. Civ. Struct. Health Monit.* **2015**, *5*, 221.

[15] C. Büttner, E. Niederleithinger, S. Buske, C. Friedrich, *J. Nondestr. Eval.* **2021**, *40*, 99.
[16] K. Dugmore, D. Jonson, M. Walker, *Compos. Struct.* **2002**, *58*, 601.
[17] E. N. Landis, E. Hassefras, T. S. Oesch, E. Niederleithinger, *Constr. Build. Mater.* **2021**, *268*, 121124.
[18] J. Krautkrämer, H. Krautkrämer, in *Ultrasonic Testing of Materials*, book section 15, Springer, Berlin, Heidelberg, Germany **1990**, pp. 266–278.
[19] C. Klinger, D. Bettge, *Eng. Fail. Anal.* **2013**, *35*, 66.
[20] M. A. Goñi, C.-E. Rousseau, *Ultrasonics* **2014**, *54*, 544.
[21] T. Terzioglu, M. M. Karthik, S. Hurlebaus, M. B. D. Hueste, S. Maack, J. Woestmann, H. Wiggenhauser, M. Krause, P. K. Miller, L. D. Olson, *NDT E Int.* **2018**, *99*, 23.
[22] Q. Wang, K. Attenborough, S. Woodhead, *J. Sound Vib.* **2000**, *236*, 781.
[23] R. G. Maev, R. E. Green, A. M. Siddiolo, *Res. Nondestruct. Eval.* **2006**, *17*, 191.
[24] J. Pierre, F. Elias, V. Leroy, *Ultrasonics* **2013**, *53*, 622.
[25] R. Kazys, V. Vaskeliene, *Sensors* **2021**, *21*, 3200.
[26] D. E. Chimenti, *Ultrasonics* **2014**, *54*, 1804.
[27] B. Gräfe, Doctoral thesis, Technische Universität Berlin, Germany, **2009**.
[28] T. E. Gomez Alvarez-Arenas, *IEEE Trans. Ultrason. Ferroelectr. Freq. Control* **2004**, *51*, 624.
[29] V. T. Rathod, *Sensors* **2020**, *20*, 4051.
[30] M. Daschewski, R. Boehm, J. Prager, M. Kreutzbruck, A. Harrer, *J. Appl. Phys.* **2013**, *114*, 1.
[31] J. Song, Y. Li, Y. Li, G. Liu, *J. Appl. Phys.* **2018**, *124*, 164902.
[32] D. Kotschate, M. Gaal, H. Kersten, *Appl. Phys. Lett.* **2018**, *112*, 1.
[33] D. Kotschate, S. Wendland, M. Gaal, in *Proc. 10th Int. Symp. NDT Aerosp.*, vol. *168*, DGZfP, Berlin, Germany **2018**, pp. 1–7.
[34] K. Y. Kim, W. Sachse, *Appl. Phys. Lett.* **1983**, *43*, 1099.
[35] T. Tran, P. Samant, L. Xiang, Y. Liu, in *Proc. IMECE2019*, vol. *1*, ASME, New York **2019**, pp. 1–5.
[36] B. Hosten, P. A. Bernard, *J. Acoust. Soc. Am.* **1998**, *104*, 860.
[37] E. Guilliorit, B. Hosten, C. Bacon, D. E. Chimenti, *Ultrasonics* **2003**, *41*, 97.
[38] D. A. Hutchins, in,*Physical Acoustics*, vol. *18*, book section 2, Academic Press, San Diego, CA, USA **1988**, pp. 21–123.
[39] S.-C. Hong, A.-D. Abetew, J.-R. Lee, J.-B. Ihn, *Opt. Lasers Eng.* **2017**, *99*, 58.
[40] B. Bühling, C. Strangfeld, S. Maack, T. Schweitzer, *J. Acoust. Soc. Am.* **2021**, *149*, 2150.
[41] T. Schweitzer, M. Hörmann, B. Bühling, B. Bobusch, *Fluids* **2021**, *6*, 171.
[42] D. W. Choi, C. McIntyre, D. A. Hutchins, D. R. Billson, *Ultrasonics* **2002**, *40*, 145.
[43] S. H. Lessly, S. Rajendran, *Nondestr. Test. Eval.* **2022**, *37*, 134.
[44] B. B. Beeken, *Fluidics Quarterly* **1973**, *5*, 18.
[45] K. Srinivasan, T. Sundararajan, S. Narayanan, T. J. S. Jothi, *Appl. Acoust.* **2009**, *70*, 1061.
[46] J. M. Kirshner, R. Gottron, Fluerics 28: State-of-the-art, Harry Diamond Laboratories, **1969**, Report No. AD703117.
[47] B. C. Bobusch, Doctoral thesis, Technische Universität Berlin, Germany, **2015**.
[48] D. Bain, *Heavy Current Fluidics: Course held at the Department of Fluiddynamics, October 1970*, Springer Vienna, Vienna **1970**.
[49] J. W. Joyce, Fluidics: Basic components and applications, Harry Diamond Laboratories, **1983**, Report No. ADA134046.
[50] H. L. Fox, *Fluidics Quarterly* **1967**, *21*, 38.
[51] J. R. Tippetts, G. H. Priestman, D. Thompson, *J. Dyn. Syst., Meas., Control* **1981**, *103*, 342.
[52] W. J. Westerman, in *Proceedings of the Fluidics State-of-the-Art Symposium*, vol. *4*, Harry Diamond Laboratories, Washington D. C **1974**, pp. 361–391.
[53] M. Epstein, *J. Basic Eng.* **1971**, *93*, 55.
[54] B. Bühling, S. Maack, T. Schweitzer, C. Strangfeld, *Ultrasonics* **2022**, *119*, 106612.
[55] S. Caporale, S. Callegari, D. A. Hutchins, S. Laureti, P. Burrascano, M. Ricci, in *Ultrasonic Nondestructive Evaluation Systems: Industrial Application Issues*, book section 4, Springer International Publishing, Cham, Switzerland **2015**, pp. 85–140.
[56] V. L. Newhouse, E. S. Furgason, N. M. Bilgutay, G. R. Cooper, in *IEEE Ultrason. Symp.*, IEEE, New York, NY, USA **1974**, pp. 712–715.
[57] E. S. Furgason, V. L. Newhouse, N. M. Bilgutay, G. R. Cooper, *Ultrasonics* **1975**, *13*, 11.
[58] D. Hutchins, P. Burrascano, L. Davis, S. Laureti, M. Ricci, *Ultrasonics* **2014**, *54*, 1745.
[59] S. Laureti, M. Ricci, M. N. I. B. Mohamed, L. Senni, L. A. J. Davis, D. A. Hutchins, *Ultrasonics* **2018**, *85*, 31.
[60] D. A. Hutchins, R. L. Watson, L. A. J. Davis, L. Akanji, D. R. Billson, P. Burrascano, S. Laureti, M. Ricci, *Sensors* **2020**, *20*, 2285.
[61] B. Bühling, S. Maack, C. Strangfeld, *Appl. Acoust.* **2022**, *189*, 108608.
[62] B. Bühling, S. Küttenbaum, S. Maack, C. Strangfeld, *Sensors* **2022**, *22*, 6.
[63] T. Ehrhart, R. Steiger, A. Frangi, *Eur. J. Wood Wood Prod.* **2018**, *76*, 925.
[64] M. O. Culjat, D. Goldenberg, P. Tewari, R. S. Singh, *Ultrasound Med. Biol.* **2010**, *36*, 861.
[65] B. Meirza, H. Hasegawa, M. Evertsson, S. Sjöstrand, M. Cinthio, in *Proc. IEEE IUS*, IEEE, New York, NY, USA **2019**, pp. 1209–1211.
[66] A. T. Peek, C. Hunter, W. Kreider, T. D. Khokhlova, P. B. Rosnitskiy, P. V. Yuldashev, O. A. Sapozhnikov, V. A. Khokhlova, *J. Acoust. Soc. Am.* **2020**, *148*, 3569.
[67] L. Al-Zogbi, B. Bock, S. Schaffer, T. Fleiter, A. Krieger, *Ultrasound Med. Biol.* **2021**, *47*, 820.
[68] S. Maack, Doctoral thesis, Technische Universität Berlin, Germany, **2012**.
[69] M. Grohmann, S. Müller, E. Niederleithinger, S. Sieber, *Near Surf. Geophys.* **2017**, *15*, 242.
[70] I. Coelho Lima, M. Grohmann, E. Niederleithinger, in *DGZfP Jahrestagung 2018*, DGZfP, Berlin, Germany **2018**, pp. 1–10.
[71] B.-C. Kim, J.-Y. Kim, *Mech. Res. Commun.* **2009**, *36*, 207.
[72] V. Bucur, *IAWA J.* **1988**, *9*, 67.
[73] V. Bucur, in *Acoustics of Wood*, book section 4, Springer, Berlin, Heidelberg, Germany **2006**, pp. 39–104.
[74] A. G. M. Hasenstab, Doctoral thesis, Technische Universität Berlin, Germany, **2006**.
[75] Q. Zhu, C. Burtin, C. Binetruy, *Polym. Test.* **2014**, *40*, 178.
[76] S. Sjöstrand, B. Meirza, L. Grassi, I. Svensson, L. C. Camargo, T. Z. Pavan, M. Evertsson, *Ultrasound Med. Biol.* **2020**, *46*, 2070.
[77] P. Purnell, T. H. Gan, D. A. Hutchins, J. Berriman, *Cem. Concr. Res.* **2004**, *34*, 1185.
[78] J. Berriman, P. Purnell, D. A. Hutchins, A. Neild, *Ultrasonics* **2005**, *43*, 211.
[79] M. Schickert, M. Krause, in *Non-Destructive Evaluation of Reinforced Concrete Structures*, vol. *2*, book section 22, Woodhead Publishing, Cambridge, UK **2010**, pp. 490–530.
[80] V. Bucur, F. Feeney, *Ultrasonics* **1992**, *30*, 76.
[81] M. Megan, S. Adam, C. George, C. B. Frank, R. Henrique, in *Proc. SPIE*, vol. *7981*, SPIE, Bellingham, WA, USA **2011**, pp. 1–13.
[82] N. Levanon, E. Mozeson, *Radar Signals*, John Wiley & Sons, Inc, Hoboken, NJ, USA **2004**.
[83] B. Bühling, T. Schweitzer, S. Maack, C. Strangfeld, in *Fortschritte der Akustik – DAGA 2021*, DEGA, Berlin, Germany **2021**, pp. 48–51.
[84] A. Torras-Rosell, Doctoral thesis, Technical University of Denmark, Kongens Lyngby, Denmark, **2014**.